



# Holocene lowering of the Laurentide ice sheet affects North Atlantic gyre circulation and climate

Lauren J. Gregoire<sup>1</sup> · Ruza F. Ivanovic<sup>1</sup> · Amanda C. Maycock<sup>1</sup> · Paul J. Valdes<sup>2</sup> · Samantha Stevenson<sup>3</sup>

Received: 29 March 2017 / Accepted: 19 December 2017 / Published online: 6 February 2018  
© The Author(s) 2018. This article is an open access publication

## Abstract

The Laurentide ice sheet, which covered Canada during glacial periods, had a major influence on atmospheric circulation and surface climate, but its role in climate during the early Holocene (9–7 ka), when it was thinner and confined around Hudson Bay, is unclear. It has been suggested that the demise of the ice sheet played a role in the 8.2 ka event (an abrupt 1–3 °C Northern Hemisphere cooling lasting ~ 160 years) through the influence of changing topography on atmospheric circulation. To test this hypothesis, and to investigate the broader implications of changing ice sheet topography for climate, we analyse a set of equilibrium climate simulations with ice sheet topographies taken at 500 year intervals from 9.5 to 8.0 ka. Between 9.5 and 8.0 ka, our simulations show a 2 °C cooling south of Iceland and a 1 °C warming between 40° and 50°N in the North Atlantic. These surface temperature changes are associated with a weakening of the subtropical and subpolar gyres caused by a decreasing wind stress curl over the mid-North Atlantic as the ice sheet lowers. The climate response is strongest during the period of peak ice volume change (9.5–8.5 ka), but becomes negligible after 8.5 ka. The climatic effects of the Laurentide ice sheet lowering during the Holocene are restricted to the North Atlantic sector. Thus, topographic forcing is unlikely to have played a major role in the 8.2 ka event and had only a small effect on Holocene climate change compared to the effects of changes in greenhouse gases, insolation and ice sheet meltwater.

**Keywords** Ice sheet topography · Holocene · Atmospheric circulation · Wind driven Ocean circulation · Laurentide Ice sheet · 8.2 kyr event

## 1 Introduction

Ice sheet topography has been shown to have a large impact on glacial climate. Topographic changes can influence atmospheric circulation through interactions with atmospheric stationary waves (Cook and Held 1988; Hoskins and Karoly 1981; Löffverström et al. 2016; Valdes and Hoskins 1991) and storm tracks (Li and Battisti 2008). These mechanisms account for most of the changes in atmospheric circulation at the Last Glacial Maximum (LGM, 21,000 years ago; 21 ka), in comparison to the smaller effects of

differences in greenhouse gas concentrations and changes in sea ice extent (Pausata et al. 2011). Specifically, the presence of the large Laurentide ice sheet (LIS) in North America at the Last Glacial Maximum produced a stronger and more zonal jet stream (Hall et al. 1996; Kageyama and Valdes 2000; Löffverström and Lora 2017), though North Atlantic storminess may have been lower than today (Li and Battisti 2008). During glacial-interglacial periods, the LIS influence on stationary waves impacted European climate (Kageyama and Valdes 2000; Li and Battisti 2008; Liakka et al. 2016; Löffverström et al. 2016), affecting the growth and retreat of the Eurasian ice sheet (Beghin et al. 2015; Liakka et al. 2016; Löffverström et al. 2014). In turn, changes in atmospheric circulation can affect North Atlantic gyre circulation and the Atlantic Meridional Overturning Circulation (Gong et al. 2015).

Changes in ice sheet topography can also affect climate on sub-millennial to millennial timescales. For example, during Heinrich events, the enhanced discharge of icebergs from the LIS into the North Atlantic was accompanied by

✉ Lauren J. Gregoire  
l.j.gregoire@leeds.ac.uk

<sup>1</sup> School of Earth and Environment, University of Leeds, Leeds LS2 9JT, UK

<sup>2</sup> School of Geographical Sciences, University of Bristol, Bristol BS8 1SS, UK

<sup>3</sup> Earth Research Institute, University of California Santa Barbara, Santa Barbara, CA 93106-3060, USA

a lowering of the ice sheet around Hudson Bay. This ice sheet lowering is thought to have produced relatively rapid changes in regional climate, including a warmer and wetter Florida and a warmer central North Atlantic (Hostetler et al. 1999; Roberts et al. 2014). Lowering of the LIS over glacial-interglacial cycles may even control abrupt climate changes during Dansgaard–Oeschger events (Zhang et al. 2014), when rapid multi-decadal scale warming of several degrees precedes more gradual cooling and a return to glacial climates in the Northern Hemisphere.

At the start of the Holocene (9 ka), remnants of the LIS, which during the LGM covered the whole of Canada reaching as far south as the Great Lakes, still existed in the Hudson Bay region. Little is known about the potential impacts of the remnants of the LIS on climate during the early Holocene (9–7 ka), the start of the current interglacial period. It has, however, been hypothesised that the changes in topography that accompanied the LIS demise may have played a role in the 8.2 ka event, an abrupt Northern Hemisphere surface cooling of up to 3 °C and associated weakening of Atlantic Meridional Overturning Circulation that took place over ~160 years (Hillaire-Marcel et al. 2007). Traditionally, the 8.2 ka event was thought to have been caused by sudden drainage of proglacial Lakes Agassiz and Ojibway, releasing 163,000 km<sup>3</sup> of water into the North Atlantic within a couple of years (Teller et al. 2002). More recently, Gregoire et al. (2012) suggested there were rapid changes in the volume and extent of the LIS between 9 and 8 ka associated with the separation of ice domes around Hudson Bay. Renssen et al. (2009, 2010) showed that meltwater associated with early Holocene deglaciation can have an important impact on the North Atlantic circulation, and Matero et al. (2017) have shown that the meltwater input to the North Atlantic from the ice dome separation disrupts the Atlantic Meridional Overturning Circulation, producing a surface climate signal that matches the spatial pattern, magnitude and duration of the 8.2 ka event from proxy data.

However, given that this period also coincided with abrupt changes in the topography of the LIS, the question is raised: what impact did topographical changes during the early Holocene have on the climate, and did this mechanism play a role in the 8.2 ka event? A related question, motivated by previous work (Liakka 2012; Liakka et al. 2012; Löfverström et al. 2014, 2016), is: do the climatic effects of changing ice sheet topography vary linearly with the changes in ice sheet size? This is important to address, since although the LIS was considerably smaller by the early Holocene compared to at the LGM, it has been suggested that changes in ice sheet topography may have been important for driving regional climate variations over this period (Hillaire-Marcel et al. 2007).

Here, we evaluate the effect of changes in the LIS topography on the evolution of climate over the early Holocene

and, for the first time, we test its role in the 8.2 ka event. To do this, we analyse a series of climate model simulations of the early Holocene period (9.5–8.0 ka) forced with ice sheet topography taken from a dynamical ice sheet model. The simulations differ only in their representation of ice sheet topography over North America in order to isolate this effect from other forcings such as changes in greenhouse gases, orbit and ice sheet meltwater. We further assess the linearity of the climatic response to successive approximately linear changes in ice sheet elevation through time.

## 2 Methods

We ran a series of experiments with the Met Office Hadley Centre Coupled Model version 3 (HadCM3) ocean–atmosphere–vegetation general circulation model (Cox 2001; Gordon et al. 2000; Pope et al. 2000; Valdes et al. 2017). The atmosphere has a regular latitude-longitude grid of 2.5° × 3.75° resolution and 19 hybrid sigma-pressure coordinate layers, from the surface up to ~10 hPa. The ocean has a horizontal resolution of 1.25° × 1.25° with 20 vertical layers. The dynamic vegetation model TRIFFID (Top-down Representation of Interactive Foliage and Flora Including Dynamics) is connected to the land surface scheme MOSES 2.1 (Met Office Surface Exchange Scheme) and coupled within the atmospheric general circulation model. This model has been extensively used to model past climates (e.g. Lunt et al. 2008; Roberts et al. 2014; Ivanovic et al. 2014, 2017; Singarayer et al. 2011; Valdes et al. 2017). and performs well with respect to mean climate (Flato et al. 2013), capturing the key features of the mid-latitude atmospheric circulation, including planetary waves and storm tracks (Valdes et al. 2017). Furthermore, its computational efficiency allows us to perform the long (multi-centennial) experiments needed to simulate equilibrium climates different from today and evaluate coupled atmosphere–ocean responses.

Our experiments build on the 9.0 ka equilibrium climate simulation of Singarayer et al. (2011). This simulation is forced with the orbital configuration of 9.0 ka (Berger and Loutre 1991). The greenhouse gas concentrations are set to 265 parts per million by volume (ppmv) for CO<sub>2</sub> (Petit et al. 1999), 666 parts per billion by volume (ppbv) for CH<sub>4</sub> (Loulergue et al. 2008), and 259 ppbv for N<sub>2</sub>O (Spahni et al. 2005) based on the EPICA (European Project for Ice Coring in Antarctica) Dome C ice core chronology EDC3 (Parrenin et al. 2007). Finally, the topography, land-sea mask, bathymetry and ice sheet extent are based on ICE-5G (VM2; henceforth ‘ICE-5G’) reconstruction (Peltier 2004). This simulation was initially spun-up for 1000 years, then continued for an additional 750 years with dynamical vegetation, providing the initial conditions for our experiments.

Starting from the end of the spin-up simulation, we run four 500 year-long simulations. These are each forced with a snapshot of the LIS elevation and extent modelled by Gregoire et al. (2012) at 9.5, 9.0, 8.5 and 8.0 ka, respectively (Fig. 1). These dates were chosen to span the separation of ice sheet domes around Hudson Bay; the so-called ‘Hudson Bay saddle collapse’ (Gregoire et al. 2012). In order to isolate the climatic impact of the topography and albedo changes associated with the Hudson Bay saddle collapse, the simulations presented here include only topographical changes in the ice sheet and surface albedo changes due to the evolution of ice sheet extent, but do not include any meltwater fluxes into the ocean. The effects of the freshwater discharge associated with the Hudson Bay saddle collapse are described in detail by Matero et al. (2017) and are therefore not considered further in this study.

We apply changes in ice sheet topography as anomalies to the ICE-5G orography included in the 9 ka spin-up simulation. To do this, we first regrid the ice sheet extent and surface elevation model output of Gregoire et al. (2012) at 9.5, 9.0, 8.5 and 8.0 ka from the 40 km Cartesian ice sheet model grid onto the 1° regular latitude-longitude grid of ICE-5G using a nearest neighbour method. We then extract the ice extent and topography over the LIS region (120°W–50°W, 40°N–75°N; Fig. 1). These data are used to create the model boundary conditions for ice mask, orography and river routing using the same method as Singarayer and Valdes (2010). With the exception of changes in ice sheet topography and ice extent, which affects surface albedo, all other boundary conditions are identical in the four experiments (including land-sea mask, bathymetry and river routing). We compare the 9.5 ka experiments with a 0.0 ka climate simulation (equivalent to a pre-industrial control simulation with boundary conditions changed accordingly) continued for a further 500 years from the 0 ka simulation performed by Singarayer et al. (2011). All climate means and standard deviations are calculated over the last 100 years of the simulations to allow the model to equilibrate to any altered boundary conditions. Input data and climatological means of the output of these simulations are openly available from the University of Leeds Data Repository. <https://doi.org/10.5518/305>.

### 3 Results

In the following section, we first examine the impact of LIS topography changes on climate in the early Holocene, we then describe the mechanisms linking ice sheet topography, atmospheric circulation and the North Atlantic surface ocean. Finally, we evaluate the linearity of the

climate response to step-by-step changes in the ice sheet topography between 9.5 and 8.0 ka.

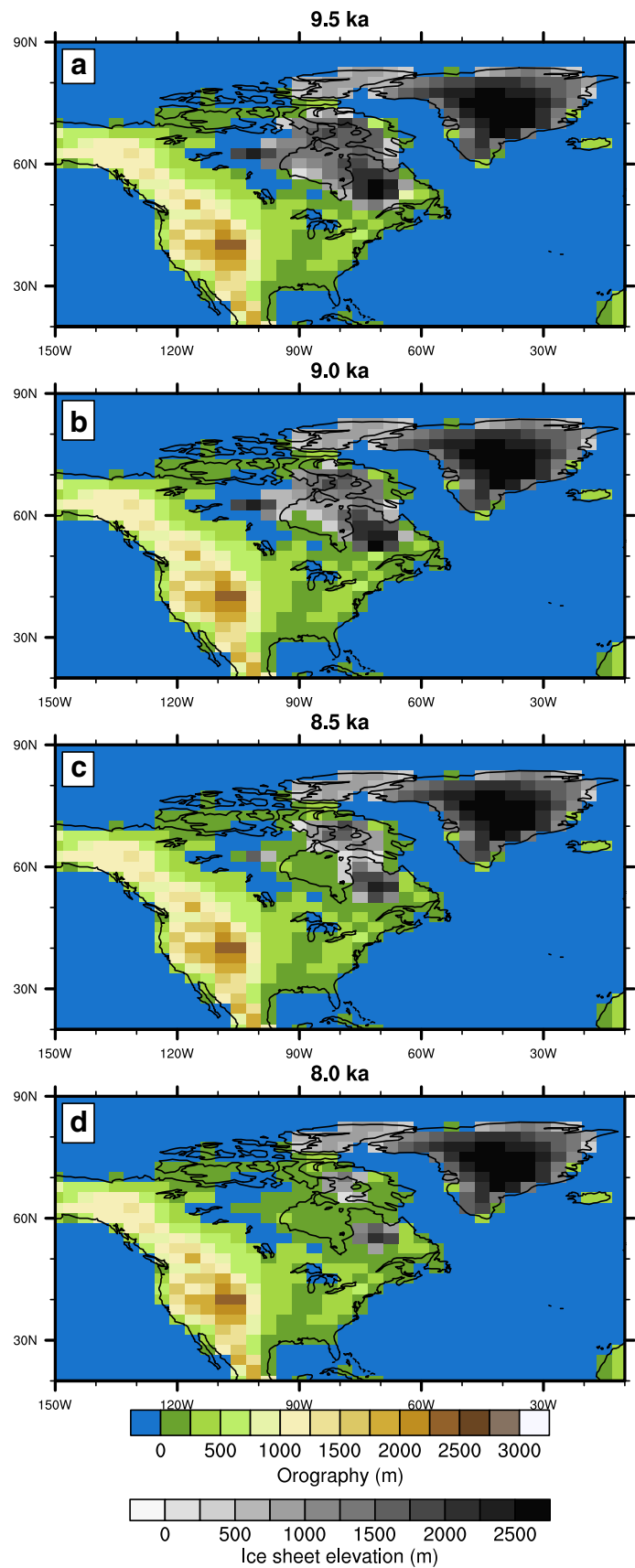
#### 3.1 Surface air temperature changes due to the 9.5–8.0 ka LIS retreat

The global mean near-surface temperature in the 9.5 ka experiment is around 0.7 °C lower than in the 0.0 ka case (Fig. 2a). This is largely in response to the higher greenhouse gas concentrations, changes in orbital parameters and the removal of the LIS in North America by 0 ka, relative to 9.5 ka. Changes in the orbit, in particular the precession (Braconnot et al. 2008), cause a strong contrast between changes in winter and summer climate, with a 2–5 °C winter warming on land (Fig. 2c) and a 1–4 °C summer cooling by 0 ka (Fig. 2e), thus reducing the amplitude of Northern Hemisphere seasonality as time passes. However, the reduction of LIS topography and ice extent since 9.5 ka also resulted in significant climate changes during the early Holocene. This can be seen in Fig. 2b, d, f, which compare the surface temperatures in the 9.5 and 8.0 ka simulations differing only in terms of the LIS topography and ice sheet extent. Note that since the ice sheet extent and thickness in our 8.0 ka experiment are small (Fig. 1d), Fig. 2b, d, f give a good indication of the contribution from ice sheet changes to the simulated differences in climate between 9.5 and 0.0 ka (Fig. 2a, c, e). This comparison shows that changes in the LIS are the dominant cause of local temperature changes during the early Holocene over north-east Canada and that they also make a substantial non-local contribution to the temperature changes over the North Atlantic and Barents Sea.

Locally over North America, the lowering and reduction in extent of the LIS between 9.5 and 8.0 ka produces a warming of up to 15 °C, due to a reduction in elevation and a decrease in surface albedo when the ice sheet retreats. The cooling produced northwest of the LIS in winter (Fig. 2d) is associated with topographically induced changes in surface winds causing a reduction in heat flux convergence to the northwest of the ice sheet as described by Löfverström et al. (2015).

In the North Atlantic, the lowering of the LIS between 9.5 and 8.0 ka alone produces a tripole pattern of surface air temperature (SAT) anomalies with: (1) a year round 1–2 °C cooling over the subpolar gyre south of Iceland; (2) a band of 1–2 °C warming between 40°N and 50°N, extending across most of the North Atlantic that is strongest in the summer; and (3) a 1 °C cooling around 30°N in winter (Fig. 2b, d, f). We discuss the cause of this signal in the following sections. The same tripole pattern of temperature change can be seen when the changes in ice sheet topography are accounted for along with changes in insolation and greenhouse gases over the early Holocene (9.5–0 ka; Fig. 2a, c, e). This suggests

**Fig. 1** Topography (colours) and ice sheet elevations (grey) in the HadCM3 simulations



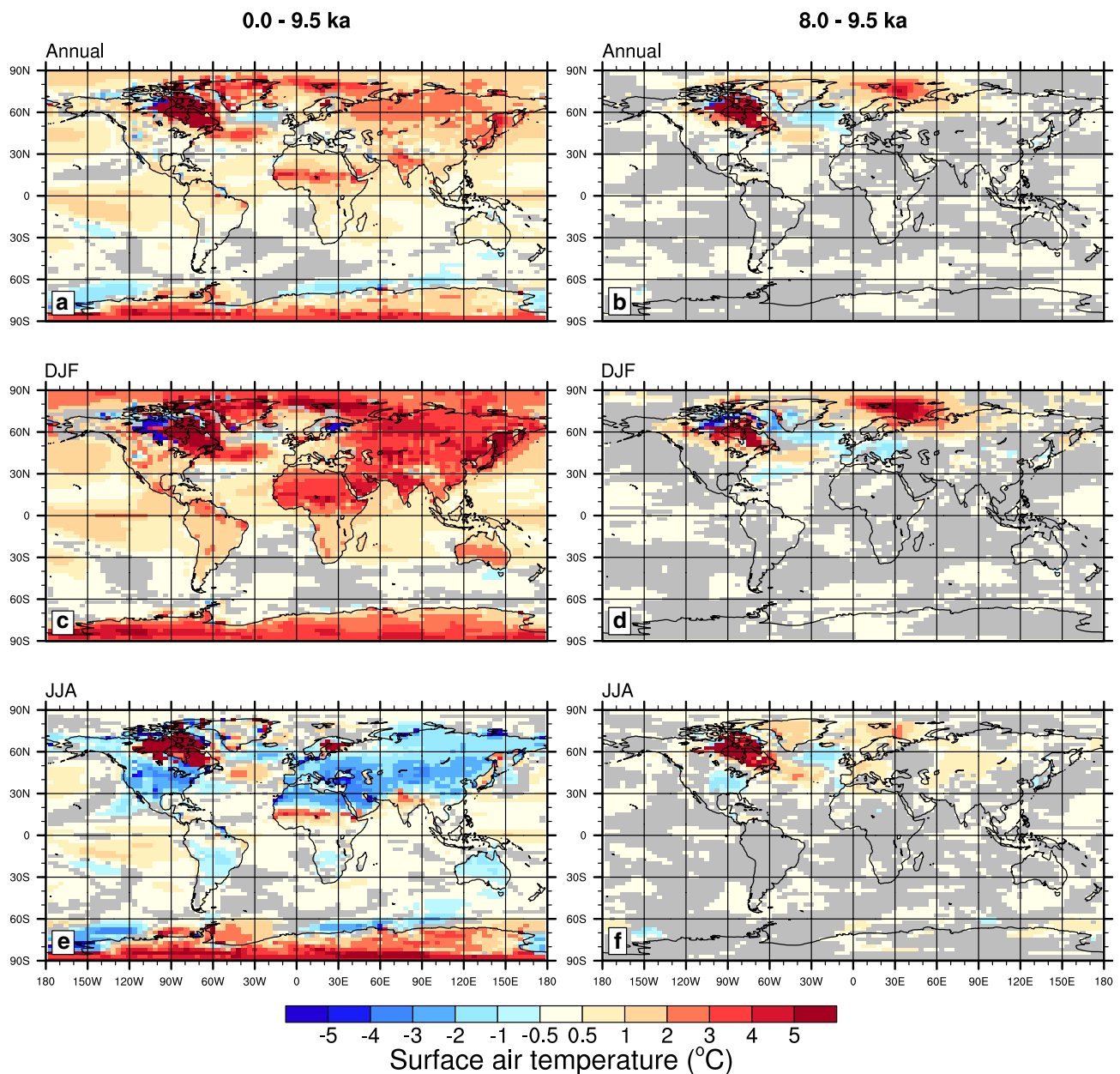


**Fig. 2** Surface air temperature differences between simulations of 0.0 ka (present day conditions) and 9.5 ka (**a, c, e**), which include the effects of ice sheet topography, orbit and CO<sub>2</sub> changes; and between simulations 8.0 and 9.5 ka (**b, d, f**), which differ only by their ice sheet topography. Annual mean (**a, b**), December–January–February

(DJF; **c, d**) and June–July–August (JJA; **e, f**) are shown. Grey shading is used over areas with less than 95% statistically significant changes using a Welch t-test with a sample size of 100 corresponding to the duration of the climatological means and standard deviation calculations

that in the North Atlantic, the effect of the ice sheet lowering is large compared to the effect of orbit and greenhouse gas forcing over this period. The ice sheet lowering between 9.5 and 8.0 ka also produces some seasonally dependent surface climate changes in Greenland, Western Europe and South of the Laurentide ice sheet (Fig. 2d, f). However, these changes are small and may be overprinted by the effects of greenhouse gases and insolation, as suggested by Figs. 2a,

c, e and 2b, d, f, which shows different pattern or directions of climate change at these locations.

In the Barents Sea, the reduction in the LIS produces a year-round warming that is strongest in boreal winter (> 5 °C) (Fig. 2d). This is associated with a reduction of sea ice (not shown), which provides a positive feedback to the initial temperature change by thermally insulating the cool air from the warm Barents Sea. While this pattern of change in the Barents Sea is a common response to changes

in ocean heat transport caused by a feedback between sea ice and circulation in the Barents Sea (e.g. Lehner et al. 2013; Semenov et al. 2009), it is worth noting that in HadCM3, this region is particularly sensitive to climate forcing under warm pre-industrial or interglacial conditions (Ivanovic et al. 2013) and the sensitivity of this response may be model dependent.

In the following sections, we investigate the impact of the imposed topographic changes on the modelled atmospheric circulation and the surface ocean to explain the mechanisms leading to the surface temperature changes described above.

### 3.2 Atmospheric circulation

The topographic forcing from the Rocky Mountains establishes a climatological stationary wave pattern consisting of an upstream ridge over the eastern North Pacific and a trough downstream over eastern North America (Held et al. 2002). In summer, there is a climatological upper level anticyclone over southern North America characteristic of a summer monsoon circulation. This large-scale stationary wave pattern is similar in all the model simulations discussed here, consistent with Löfverström et al. (2016) and Löfverström and Lora (2017), who showed that a major reorganisation of the stationary wave field only occurs in the presence of a very large LIS (e.g. at the LGM), but not for periods with smaller ice sheets similar to those in the early Holocene. Nevertheless, modest changes to the stationary wave field do occur in response to the reduction in LIS topography between 9.5 and 8.0 ka (Fig. 3). The response in the vicinity of the LIS shows a strong seasonal dependence. In winter,

the trough over eastern North America weakens and shifts slightly northwards. Conversely in summer, the trough strengthens and shifts towards the south west. Numerous studies have examined the relative roles of mechanical and thermal forcing, and their interactions, in driving the stationary wave response to North American ice sheet changes (e.g. Cook and Held 1988; Ringler and Cook 1999; Liakka 2012; Liakka et al. 2012). Mechanical forcing has been shown to be the dominant driver of stationary wave changes at the LGM (e.g. Cook and Held 1988), but thermal forcing and non-linear interactions between mechanical and thermal forcing are likely to be important for smaller more localised changes in the ice sheet (Liakka et al. 2012; Löfverström et al. 2016). However, the differences in the eddy geopotential height field in Fig. 3 show different responses in summer and winter, despite the near-surface temperature changes over the ice sheet being similar (Fig. 2d, f). This suggests that in addition to thermal forcing, mechanical forcing may also play a role in the stationary wave response, since the climatological low-level winds are stronger in winter. A detailed attribution of the changes to mechanical and thermal forcing is beyond the scope of this study.

Compared to the pre-industrial control (0 ka), the North Atlantic jet in the early Holocene (9.5 ka) is stronger, narrower and located further poleward (Fig. 4a, c). Li and Battisti (2008) found a qualitatively similar, but larger strengthening and narrowing of the North Atlantic jet structure at the LGM, when the LIS was substantially bigger. Comparing the last of our simulations (8 ka; Fig. 1d), when most of the LIS has disappeared, with the pre-industrial control (0 ka) simulation isolates the changes in the North Atlantic jet due to

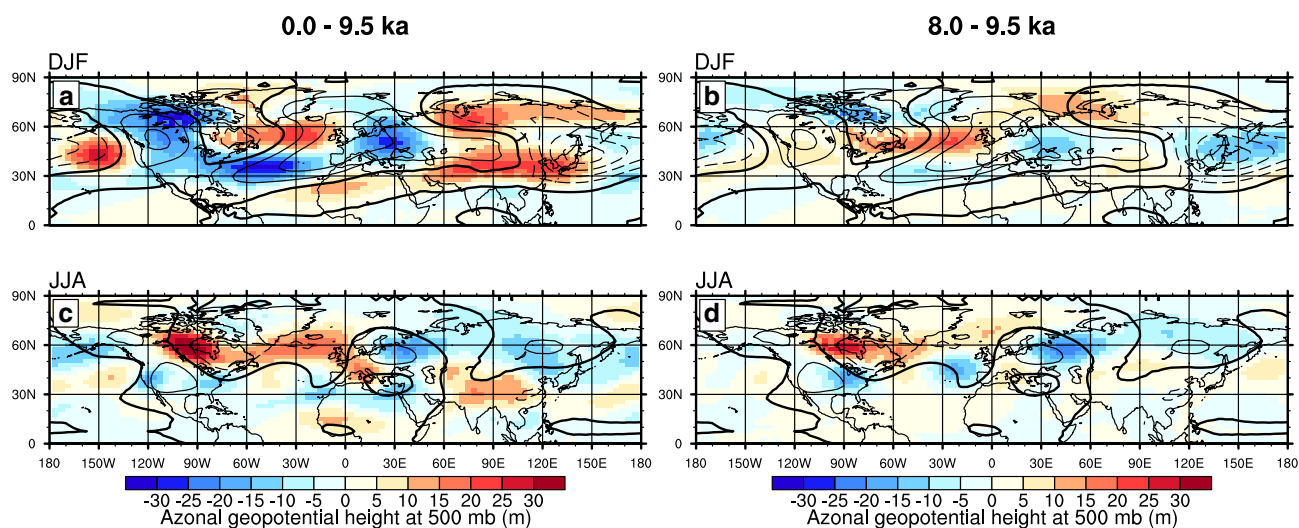


**Fig. 3** Azonal geopotential height (m) at 500 mb for the December–January–February means (DJF; **a**, **b**) and June–July–August means (JJA; **c**, **d**). Colours show difference between experiments (**a**, **c**: 0–9.5 ka; **b**, **d**: 8–9.5 ka). Contours show the relevant seasonal aver-

ages at 9.5 ka. Contours are at 50 m interval, with dashed lines for negative values, solid lines for positive values and the zero contours in bold

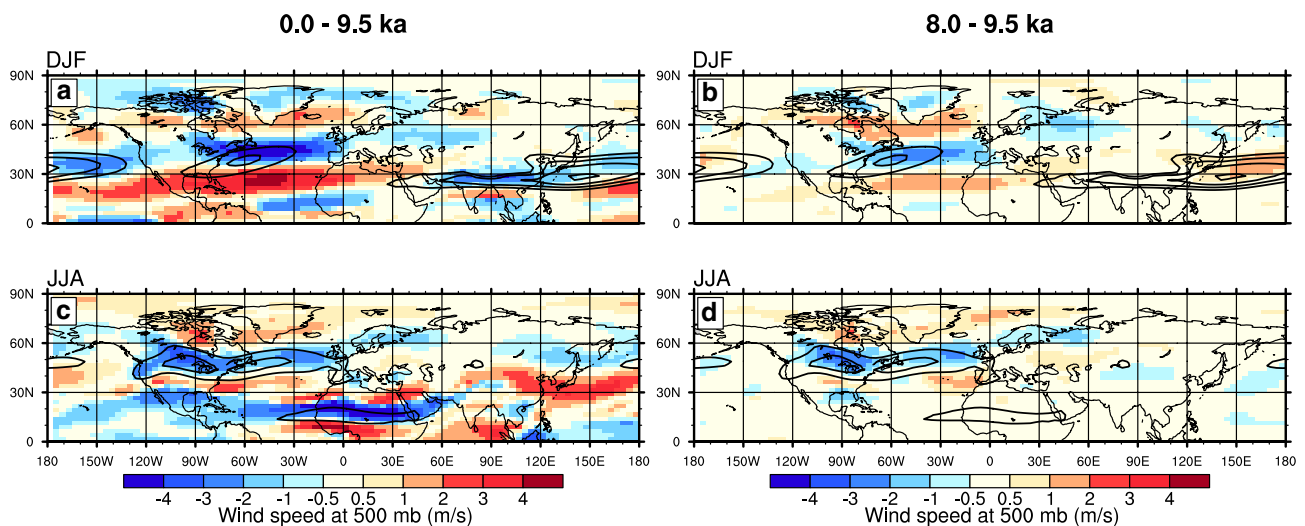


**Fig. 4** Wind speed ( $\text{m s}^{-1}$ ) at 500 mb for the December–January–February means (DJF; **a**, **b**) and June–July–August means (JJA; **c**, **d**). Contours show the relevant seasonal averages at 9.5 ka. For the DJF

means (**a**, **b**), contours start at  $20 \text{ m s}^{-1}$  with an increment of  $5 \text{ m s}^{-1}$ . For the JJA means (**c**, **d**), contours start at  $10 \text{ m s}^{-1}$  with an increment of  $5 \text{ m s}^{-1}$

greenhouse gases and orbital parameters. This reveals similar structural changes as seen in Fig. 4a, c, which suggests that changes in other forcing agents (atmospheric greenhouse gases, orbital parameters) account for the majority of the simulated changes in the North Atlantic jet between the early Holocene and present day. Hence the role of ice sheet topography alone is likely to be smaller than for the changes at the LGM (Li and Battisti 2008).

Comparing the atmospheric circulation changes between 9.5 and 8.0 ka, the climatological ridge over the North Atlantic in winter shows a wider and weaker North Atlantic eddy driven jet (Fig. 3b). The maximum 500 mb zonal wind speed in winter reduces by around  $2 \text{ m s}^{-1}$  ( $\sim 20\%$ ) (Fig. 4b). The changes in zonal winds over the North Atlantic show an equivalent barotropic structure (Fig. 5a), which suggests coupling with changes to baroclinic eddies and the storm track (c.f. Li and Battisti 2008). The changes in land-sea contrast in the western North Atlantic may alter the baroclinicity of the background environment and the associated growth of synoptic eddies. In summer, the changes in zonal wind are most pronounced upstream over the LIS and downstream near the jet exit region (Fig. 4d). These results complement earlier studies that have focused on the impact of a larger LIS at the LGM on the North Atlantic jet (e.g. Hall et al. 1996; Kageyama and Valdes 2000; Li and Battisti 2008), and reveal that changes in the eddy driven jet, albeit of a smaller amplitude, can occur for smaller changes in ice sheet topography.

### 3.3 Surface wind response drives north Atlantic gyre circulation changes

At the surface, the changes in the large-scale atmospheric flow translate into a decrease in the westerlies over the mid-North Atlantic by  $1 \text{ m s}^{-1}$  in the winter and a decrease in the subpolar easterlies off the southeast coast of Greenland (Fig. 6). This results in a winter weakening (negative anomaly) of the wind stress curl in the subpolar gyre at 8.0 ka compared to 9.5 ka (Fig. 7a). We also see a positive wind stress curl anomaly in the winter at  $40^\circ\text{N}$  along the North Atlantic drift (Fig. 7a). Wind stress curl is slightly weaker (negative anomaly) around  $30\text{--}35^\circ\text{N}$  on the western side of the Atlantic basin over the subtropical gyre. In the summer, the pattern of wind stress curl change is smaller in magnitude (Fig. 7c).

The reductions in wind stress curl cause a 13 Sv weakening ( $1 \text{ Sv} = 10^6 \text{ m}^3 \text{ s}^{-1}$ ) and slight contraction of the subpolar gyre between 9.5 and 8.0 ka, and a 10% reduction in Gulf Stream strength (from 84 to 76 Sv; calculated as the meridional transport at  $35^\circ\text{N}$  integrated over  $80^\circ\text{--}60^\circ\text{W}$  and 0–1000 m) associated with a weakening of the subtropical gyre (Fig. 8). The western boundary current flow also weakens off the coast of Florida (Fig. 8). This latter, local effect is seen by Vellinga et al. (2002), who found that it is the result of a reduction in bottom pressure torque caused by the interaction between vertical velocity at the seafloor and ocean bathymetry. It is worth noting here that there are some numerical artefacts in the ocean component of the model that could complicate the interpretation of the barotropic stream function (see “Appendix”). This affects the calculation of the absolute strength of the subpolar

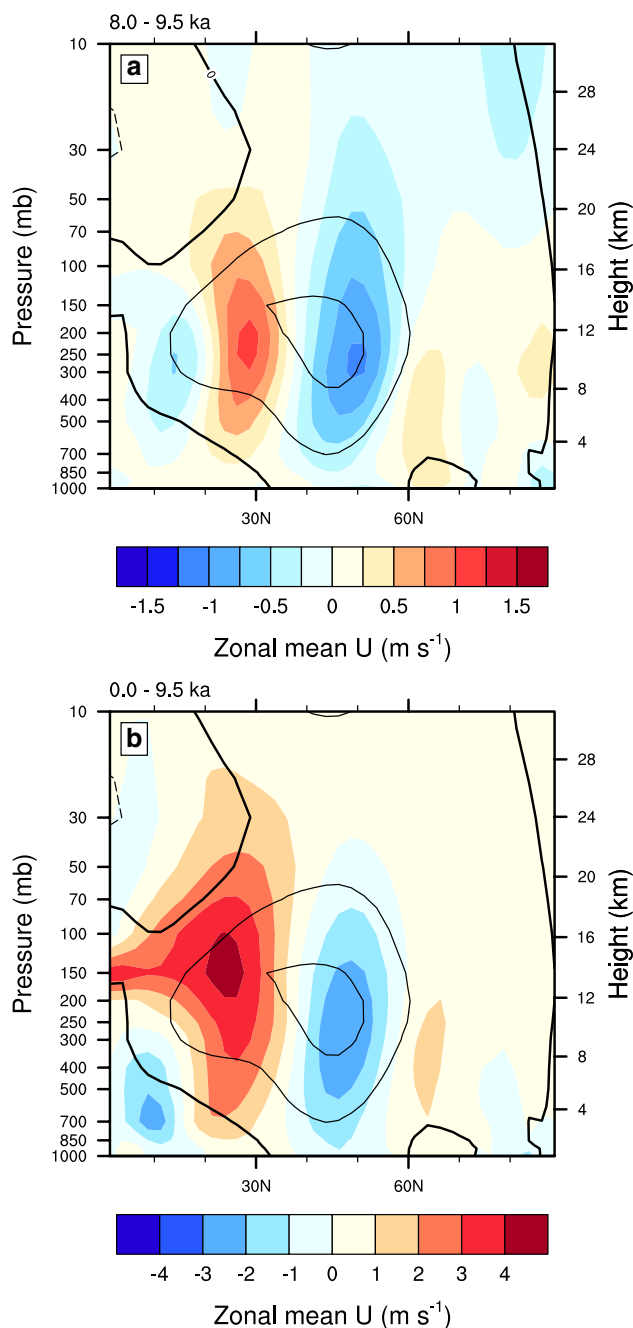


**Fig. 5** Latitude-height contour plot of the annual mean zonal component of the wind ( $U$ ) averaged between  $60^{\circ}\text{W}$  and  $0^{\circ}$  longitudes. Colours show the difference between experiments (**a**: 8–9.5 ka; **b** 0–9.5 ka) and contours show the absolute annual mean at 9.5 ka

gyre and Gulf Stream strength, although the changes in the barotropic stream function display a coherent large scale pattern of weakening of the subpolar gyre (Fig. 8). For robustness, we also calculate the changes in Sverdrup transport from the wind stress fields over the North Atlantic ( $0^{\circ}$ – $60^{\circ}\text{W}$ ), which are not affected by this artefact. The

Sverdrup transport represents the changes in ocean flow due to adjustments in surface winds. We calculate it as:

$$M(y) = -\frac{1}{\rho_{ref} \beta} \int_{0W}^{60W} \text{curl}_z \tau_{wind} dx, \quad (1)$$

where  $\rho_{ref}$  is the density of ocean water ( $1025 \text{ kg m}^{-3}$ ),  $\beta$  is the meridional gradient in the Coriolis parameter and  $\tau_{wind}$  is the wind stress over the ocean. With this sign convention, a positive value represents a clockwise gyre circulation. We find that the changes in wind stress over the North Atlantic induce an 11 Sv weakening of the Sverdrup transport over the subpolar gyre between 9.5 and 8.0 ka (Fig. 9c, h). This compares well with the 13 Sv weakening in the ocean barotropic stream function in the subpolar gyre (Fig. 8). Furthermore, at  $40^{\circ}\text{N}$  over the subtropical gyre, both the Sverdrup transport and the barotropic stream function weaken by 5 Sv (Figs. 8, 9c, h). The similarity of the magnitude and pattern of changes in the Sverdrup transport and barotropic stream function demonstrates that the gyre circulation changes are primarily driven by surface wind changes and that buoyancy forcings (e.g. due to temperature changes) and other ocean internal feedbacks play only a secondary role.

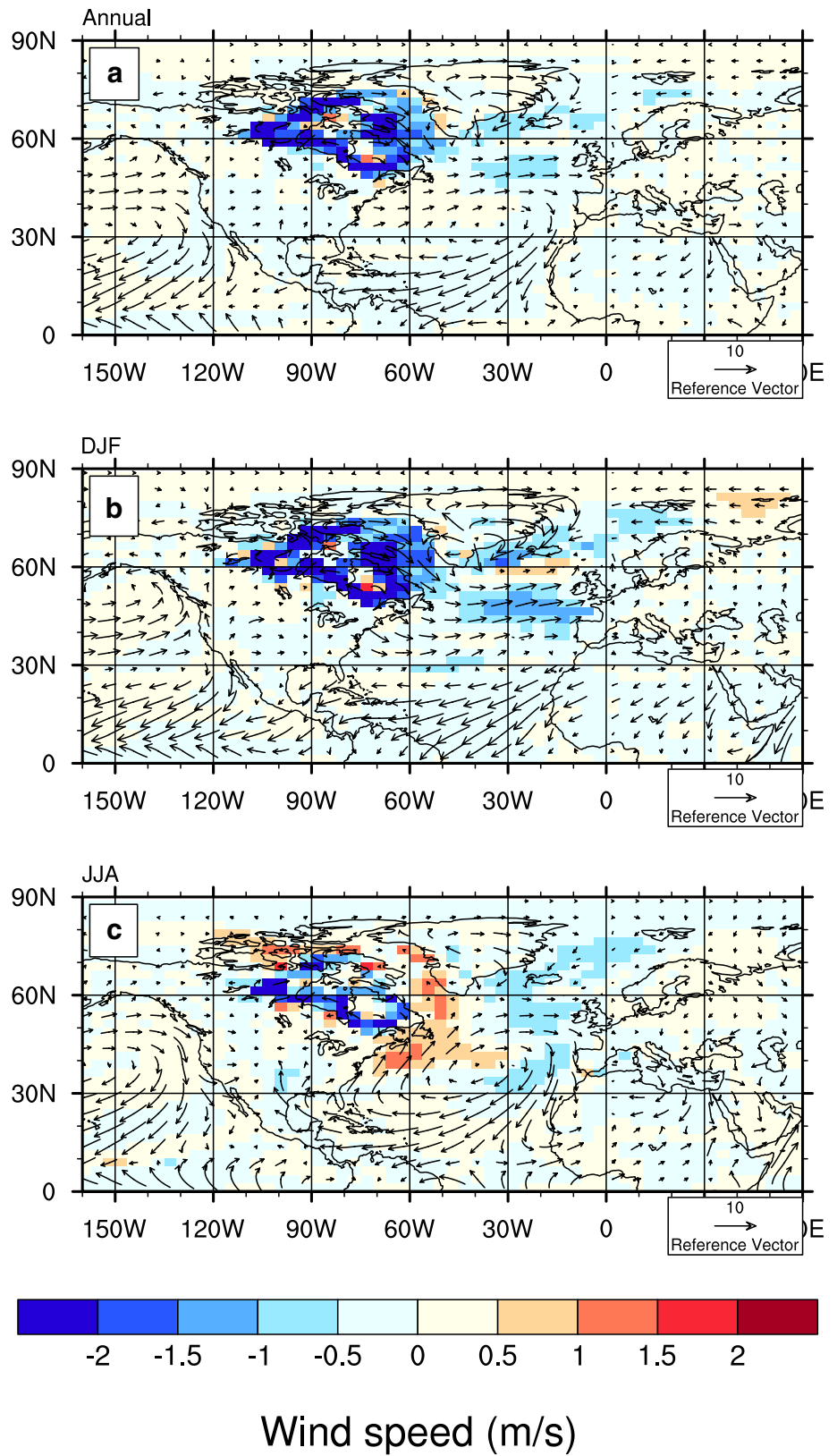
The result that a lower LIS leads to weaker surface winds and reduced North Atlantic gyre circulations and western boundary currents is consistent with the findings of Gong et al. (2015). Moreover, although their findings are based on simulations comparing the large Last Glacial Maximum ice sheet with the present day, our results show that a similar mechanism may have operated at the start of the Holocene when there was less ice and a much more modest lowering of the LIS. Furthermore, even though the presence of a large LIS can induce changes in Atlantic Meridional Overturning Circulation at the LGM (Gong et al. 2015), we find that the changes in ocean gyre circulation and surface climate between the 9.5 and 8.0 ka experiments are not associated with any significant change in Atlantic Meridional Overturning Circulation strength.

The lowering of the ice sheet also induces a weakening of the near surface anticyclonic flow over the ice sheet domes. This signal is present all year round, but particularly strong in the winter. It reduces the wind speed over the Labrador Sea. In the next section we describe how the near and far field changes in atmospheric circulation are linked to surface climate changes.

### 3.4 Link to surface climate

Over the North Atlantic, the tripole pattern in surface air temperature changes between 9.5 and 8.0 ka (Fig. 2) maps on to the changes in sea surface temperatures (Fig. 7b, d). These anomalies are strongest in the winter. In particular,

**Fig. 6** Change in 10 m wind speed from 9.5 to 8.0 ka (in  $\text{m s}^{-1}$ ) for the Annual (a), December–January–February (b) and June–July–August (c) means. Arrows show the absolute 10 m wind speed at 9.5 ka. The big differences over the ice sheet itself are a simple response to the reduction in elevation resulting in the surface being below the maximum of the jet stream



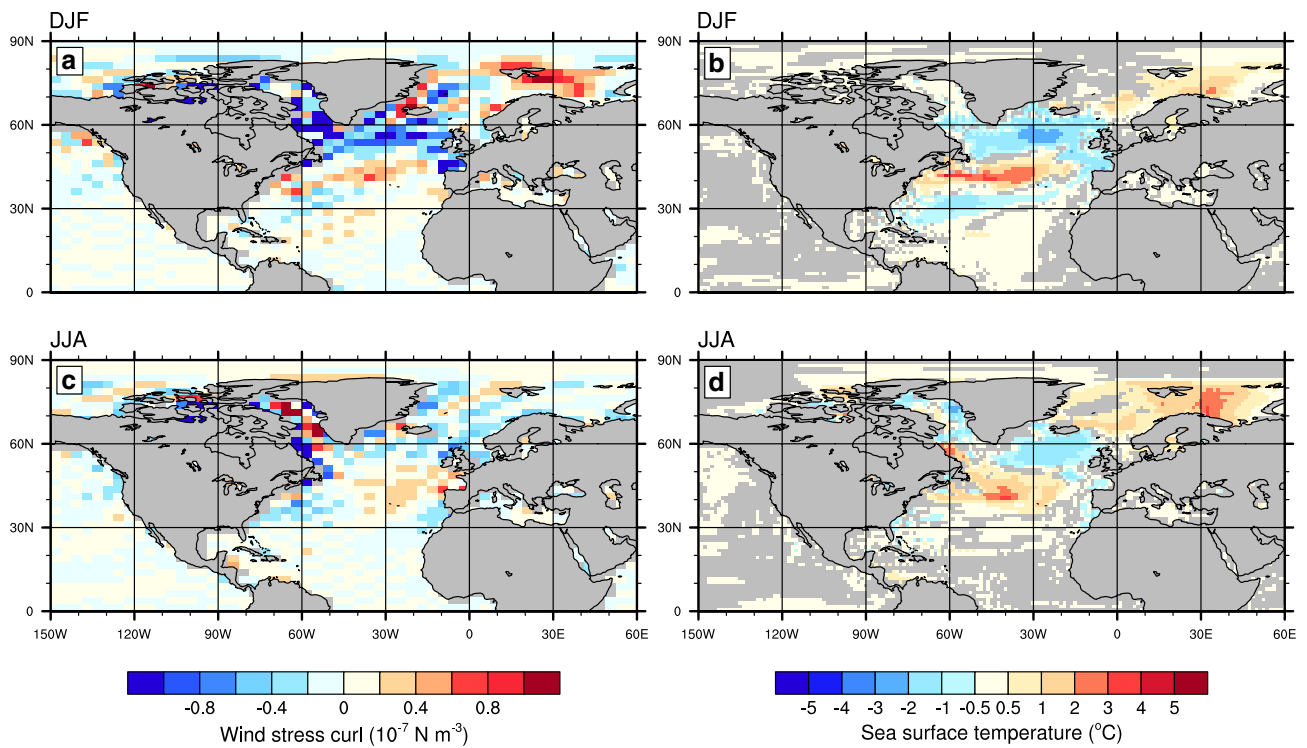


**Fig. 7** Impact of ice sheet reduction between 9.5 and 8.0 ka on the ocean surface. **a, c** The difference (8.0–9.5 ka) in wind stress curl ( $\text{N m}^{-3}$ ) over the ocean for December–January–February (DJF) and

June–July–August (JJA), respectively. **b, d** Sea surface temperature difference ( $^{\circ}\text{C}$ ) with grey shading used over areas with less than 95% statistically significant changes

**Fig. 8** Annual mean changes (8.0–9.5 ka) in ocean barotropic stream function, showing changes in gyre circulation

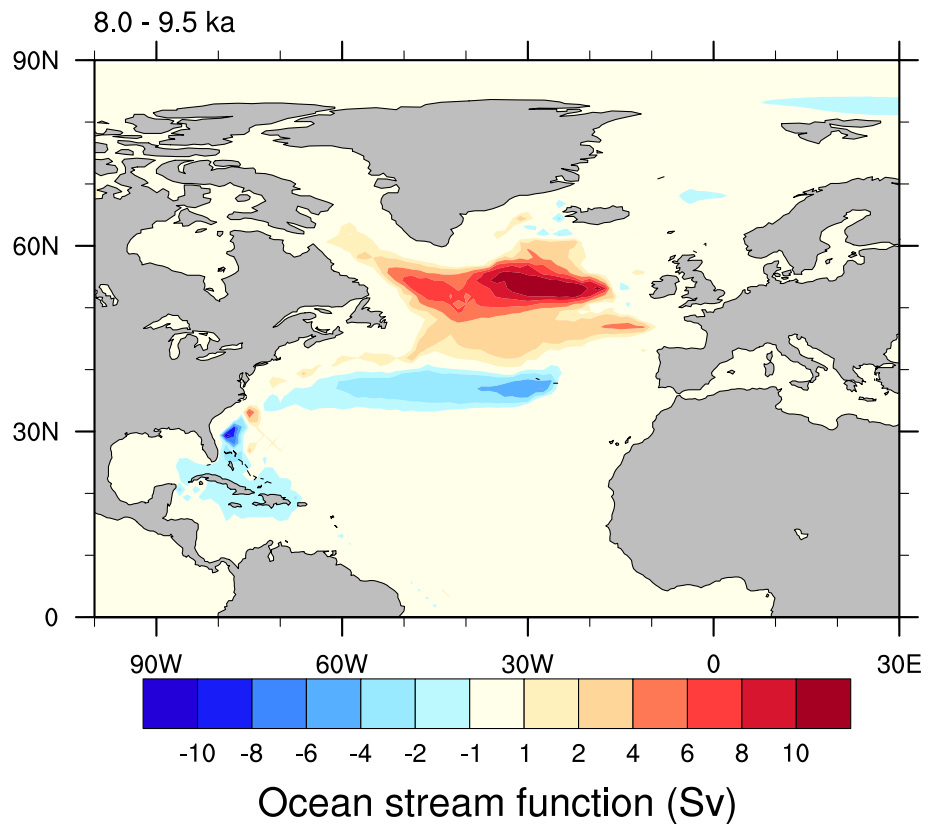


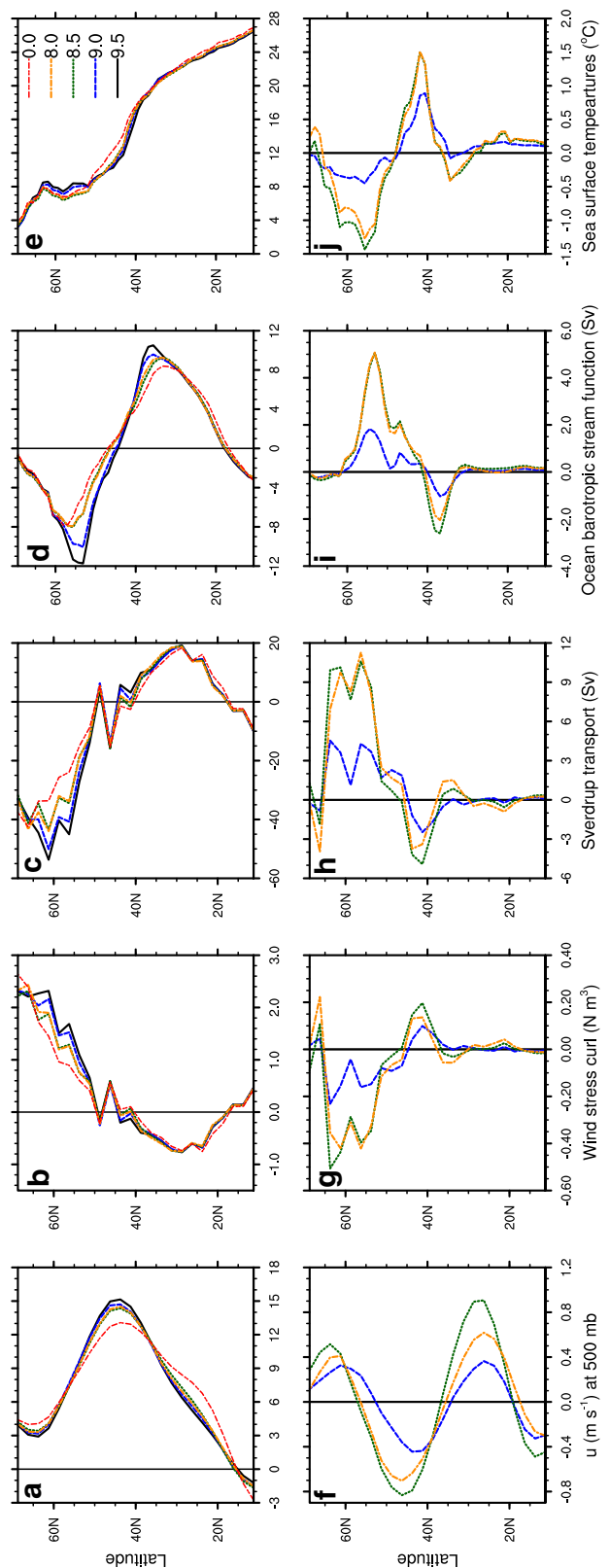
**Fig. 9** Latitudinal profiles of key climate variables over the North Atlantic (averaged or integrated between 60° and 0°W) for each time slice: **a** zonal mean of the zonal wind ( $\text{m s}^{-1}$ ) at 500 mb; **b** zonal mean surface wind stress curl ( $\text{N m}^{-3}$ ); **c** Sverdrup transport (Sv) calculated from Eq. (1), with positive values indicating clockwise gyre circulation; **d** zonal mean ocean barotropic stream function (Sv) and **e** zonal mean sea surface temperatures ( $^{\circ}\text{C}$ ). Plots **f–j** are as **a–e**, but show the differences with regards to the 9.5 ka simulation. Lines correspond to 9.5 ka (black solid line), 9.0 ka (blue dashed), 8.5 ka (green dotted line), 8.0 ka (orange dash-dot-dotted line) and 0 ka (red dash-dot-dot line)

the  $1^{\circ}\text{C}$  winter cooling around  $30^{\circ}\text{N}$  is markedly smaller in the summer.

The changes in sea surface temperature are a direct consequence of the weakening in North Atlantic gyre circulation due to a reduction in horizontal ocean heat transport. It resembles the pattern in sea surface temperatures that covaries with the North Atlantic Oscillation (e.g. Cayan 1992; Rodwell et al. 1999). The weakening of the subpolar gyre explains the dipole in sea surface temperature changes, with a  $2.5^{\circ}\text{C}$  warming of the Southern branch of the subpolar gyre (North Atlantic drift) associated with reduced southward transport of cold waters on the western side of the gyre (Figs. 7, 8) as the ice sheet lowers. The rest of the subpolar gyre cools by  $2^{\circ}\text{C}$  due to the decrease in northward transport of warm waters by its eastern branch. The weakening of the subtropical gyre and particularly the western boundary current reduces the northward transport of warm tropical water, contributing to the winter cooling in the western Atlantic at  $30^{\circ}\text{N}$ . We find no indication that the noise in the barotropic stream function (see Sect. 3.3) affects the horizontal ocean heat transport; the pattern of sea surface temperature changes is coherent and consistent with gyre circulation changes. Furthermore, although weakening of the surface winds can sometimes cause a decrease in evaporation rates, which in turn decreases latent heat flux and can increase sea surface temperatures (e.g. Xie and Philander 1994), we find that this mechanism does not operate here. Instead evaporation increases at  $40^{\circ}\text{N}$  due to the sea surface warming even with a weakening of winds. Similarly, evaporation decreases over the subpolar gyre, due to the local cooling.

The temperature changes closer to the LIS are also affected by the weakening of cold air advection from the ice sheet, as described in the previous section. In particular, this can explain the warming that occurs south of the ice sheet, over the Labrador Sea in summer, as well as off the coast of Newfoundland.

We have demonstrated here a possible link between the lowering of the LIS between 9.5 and 8.0 ka and surface climate change over and around the North Atlantic via a response in the atmospheric circulation. The next section examines the linearity of such changes with regards to ice sheet elevation.



### 3.5 Temporal evolution of climate response to early Holocene LIS demise

So far we have focussed on the equilibrium climate response to changes in LIS topography between 9.5 and 8.0 ka. We now assess the differences in climate over the North Atlantic between the successive 500 year time slice simulations.

Figure 10 shows the annual mean changes in near surface temperature between the successive time slice experiments covering 9.5–8.0 ka. There is a substantial warming over the LIS region of several degrees in all three 500 year periods along with a cooling immediately to the north of the LIS. As noted previously, the warming over the Barents Sea is related

**Table 1** Characteristics of the Laurentide ice sheet in our time slice simulations and the changes in these relative to the previous time slice

	9.5 ka	9.0 ka	8.5 ka	8.0 ka
Maximum ice sheet elevation (m)	2742	2597	2333	2040
Change		– 145	– 264	– 293
Ice area ( $10^6$ km <sup>2</sup> )	3.5	2.798	1.766	0.762
Change		– 0.702	– 1.032	– 1.004
Ice volume ( $10^6$ km <sup>3</sup> )	7.225	5.1	2.76	1.14
Change		– 2.125	– 2.34	– 1.62

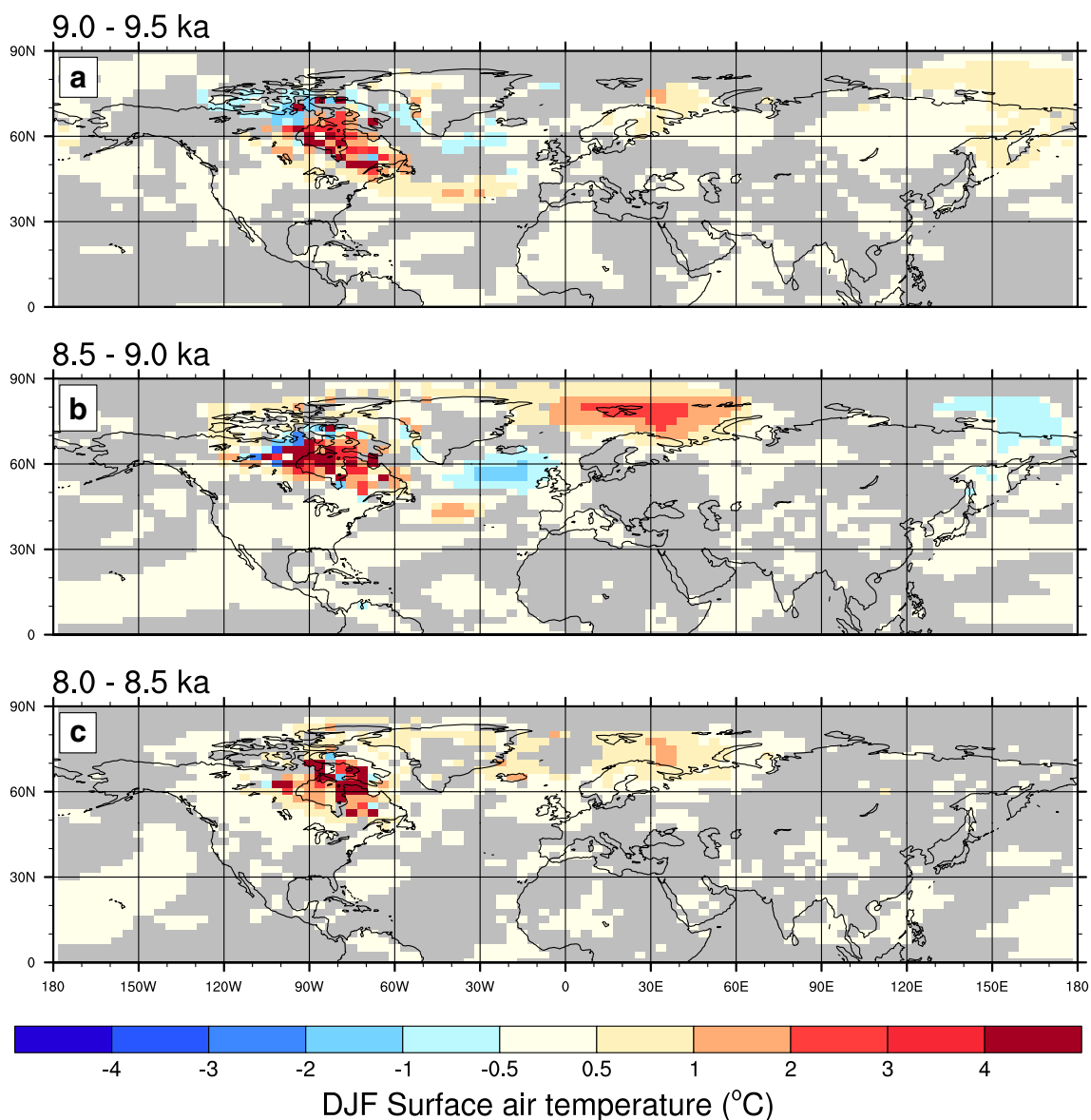


**Fig. 10** Changes in winter (December–January–February) surface air temperature (°C) between consecutive time slices; **a** 9.0–9.5 ka; **b** 8.5–9.0 ka; **c** 8.0–8.5 ka. Grey shading is used over areas with less than 95% statistically significant changes as described in Fig. 2

to sea ice changes in the simulations. Downstream over the North Atlantic the dipole pattern of temperature change discussed in Sect. 3.1, with cooling south of Iceland and warming over the mid-North Atlantic, is only found between 9.0 and 9.5 and 9.0 and 8.5 ka, with virtually no changes in this region between 8.5 and 8.0 ka despite the continued reduction in ice extent (Table 1).

To further explore the causes of these time dependent changes in North Atlantic climate in the early Holocene, Fig. 9 shows latitudinal profiles of climatological values and differences compared to 9.5 ka for 500 hPa zonal wind (a, f), near surface wind stress curl (b, g), Sverdrup transport (c, h), horizontal barotropic ocean stream function integrated over the depth of the ocean (d, i) and sea surface temperatures (e, j). As described in Sect. 3.2, the overall changes in ice topography between 9.5 and 8.0 ka lead to a weaker and wider North Atlantic jet. Between 9.5 and 9.0 ka there is a weakening in the winds near the jet maximum of around  $0.8 \text{ m s}^{-1}$  and an increase in wind on the flanks of the jet indicating a broadening. This pattern of change continues between 9.0 and 8.5 ka (compare blue and green lines in Fig. 9a, f), but the further changes between 8.5 and 8.0 ka are rather small. Thus the majority of the simulated changes in the North Atlantic jet between 9.5 and 8.0 ka occur between 9.5 and 8.5 ka.

Examining the changes in surface wind stress curl, shows that it decreases over the subpolar gyre and intensifies over the North Atlantic drift between 9.5 and 9.0 ka, leading to a dipole of sea surface temperature anomalies with a  $0.5 \text{ }^\circ\text{C}$  cooling in the subpolar gyre and a  $0.5\text{--}1 \text{ }^\circ\text{C}$  warming at  $40^\circ\text{N}$  (Fig. 9j), as seen in Fig. 7. While the ice sheet experiences large volume changes during this period ( $2.125 \times 10^6 \text{ km}^3$ ), the ice loss largely occurs on the lower parts of the ice sheet, while the ice domes remain high. Hence the changes in maximum ice sheet elevation ( $-145 \text{ m}$ ) are smaller during this period than the later ones (see Table 1).

The largest changes in wind stress curl over the North Atlantic occur between 9.0 and 8.5 ka (compare blue dashed and green dotted lines in Fig. 9b, g), inducing a further  $1 \text{ }^\circ\text{C}$  cooling south of Iceland, a further  $1 \text{ }^\circ\text{C}$  warming over the North Atlantic drift and a cooling in the subtropical gyre (Fig. 10), via changes in ocean heat transport (see Sect. 3.4). It is during this time window that the largest ice sheet changes occur, with a big reduction in ice sheet area and maximum elevation (Table 1). This corresponds to the acceleration of ice sheet melt from the ice saddle collapse mechanism described in Gregoire et al. (2012, 2016).

In all of the diagnostics considered, the changes during the last stage of ice sheet reduction (8.5–8.0 ka) are small compared to the changes between 9.5 and 8.5 ka despite the large reduction of maximum elevation changes and the continued reduction in ice extent (Table 1). This suggests that after 8.5 ka, the ice sheet has become too small to have a noticeable effect on atmospheric circulation and climate.

In short, the largest surface climate anomalies in the North Atlantic occur at the peak of ice sheet changes (9.0–8.5 ka in our model) when the reduction in maximum ice sheet elevation is large. However, when the ice sheet is small (e.g. at 8.5 ka in our model), its effect on North Atlantic surface climate becomes insignificant. This shows that the climate response is not a simple linear function of the ice volume, but is a more complex function of the detailed ice sheet geometry.

## 4 Discussion and conclusions

We ran a set of climate model simulations with different configurations of the LIS to isolate the effect of LIS changes on climate during the early Holocene from other climate drivers such as greenhouse gases and insolation. Our results show that changes in the LIS topography may have been a significant driver of changes in some aspects of North Atlantic climate during the early Holocene. We show that the lowering of the ice sheet weakens surface winds and gyre circulation in the North Atlantic, producing a cooling in the subpolar gyre, a warming at the North Atlantic drift and a cooling in the south-western part of the subtropical gyre.

Findings from previous work (e.g. Löffverström et al. 2014) suggest that when the LIS has a reduced size and shape such as during the early Holocene, it does not produce major changes in the atmospheric circulation compared to the effect of the LIS at the LGM. Our results are in line with these findings, but highlight that the LIS during the early Holocene can nonetheless produce significant, albeit small, changes in the atmospheric circulation. We also show that when these small atmospheric circulation changes interact with the ocean, it results in a weakening of the North Atlantic gyre circulation leading to significant surface temperature changes. This suggests that it is necessary to use a coupled atmosphere–ocean general circulation model to evaluate the full climate response to changes in ice sheets topography and extent.

The link between the North American ice sheet size and the strength of North Atlantic gyre circulation has also been described in another study performed with a different general circulation model in the context of glacial-interglacial ice sheet changes (Gong et al. 2015). This suggests that the mechanism described here is robust. The strengths and pattern of gyre circulation and climate response are, however, likely to be dependent on the choice of model and ice sheet topography. Factors such as the atmospheric resolution and parameterisation of gravity wave and other related model processes are likely to affect the response to LIS lowering. There are also large uncertainties in reconstructions of the topography of the Laurentide ice sheets. For example, reconstructions of LIS elevation at 9 ka differ by more than

1000 m in places (Peltier et al. 2015; Tarasov et al. 2012; Ivanovic et al. 2016). Multi-model transient simulations of the last deglaciation currently coordinated as part of the fourth phase of the Palaeoclimate Model Intercomparison Project (PMIP4; Ivanovic et al. 2016) may help further constrain the impact of ice sheet topography on climate. However, for such simulations of glacial-interglacial transitions, it is important to consider that ice sheet topography and its impact on gyre circulation evolves smoothly over thousands of years. In previous studies, the evolution of ice sheet topography has been introduced as step changes (e.g. Gregoire et al. 2015; Liu et al. 2009), but as we show here, ice sheet changes that occur on a 500 year time scale can cause significant climate changes in regions remote from the ice sheet. Therefore, prescribing such ice sheet evolution as step changes at intervals of 500–1000 years or more may introduce artificial abrupt adjustments of the atmosphere and ocean in the North Atlantic sector.

Our simulations do not include the effect of the freshwater flux released from the melting LIS into the Labrador Sea, which is thought to be the primary cause of the abrupt cooling during the 8.2 kyr event. This is assessed in detail by Matero et al. (2017), who show that the century scale acceleration in ice sheet melt caused by the Hudson Bay ice saddle collapse (the same mechanism captured here in terms of topographic changes) can explain the 160 year cooling recorded in Greenland (up to 3 °C), in the North Atlantic and in Northern Europe (1–2 °C). The effect of freshwater fluxes, therefore, have a larger impact on the surface climate (through the forced reduction in Atlantic Meridional Overturning Circulation) than the effects of ice sheet topography (and extent), which influence surface wind stress and ocean gyre circulation, but do not affect the Atlantic Meridional Overturning Circulation strength during the early Holocene. Nevertheless, while the changes in Laurentide ice sheet topography associated with the Hudson Bay ice saddle collapse are unlikely to be the

primary cause of climate change during the 8.2 kyr event, they may have influenced the patterns of surface climate changes in the North Atlantic at that time, as suggested by our results.

The evolution of ice sheet topography also operates on a longer (multi-millennial) time scale than the 8.2 kyr event. Our results suggest that, the presence of the LIS during the early Holocene (~9 ka) had a distinct effect on the climate in the North Atlantic subpolar and subtropical gyre regions compared to the effects of orbit and greenhouse gases forcings. We therefore recommend that to fully account for climate changes in simulations of the early Holocene and of the 8.2 kyr event, changes in ice sheet geometry should be included alongside other forcings.

**Acknowledgements** This work made use of the facilities of N8 HPC Centre of Excellence, provided and funded by the N8 consortium and EPSRC (Grant EP/K000225/1). The Centre is co-ordinated by the Universities of Leeds and Manchester. ACM acknowledges support from NERC Grant NE/M018199/1, PJV from NERC Grant NE/I010912/1 and RFI from NERC Grant NE/K008536/1. We also thank Anne de Vernal for the discussions that have inspired this work.

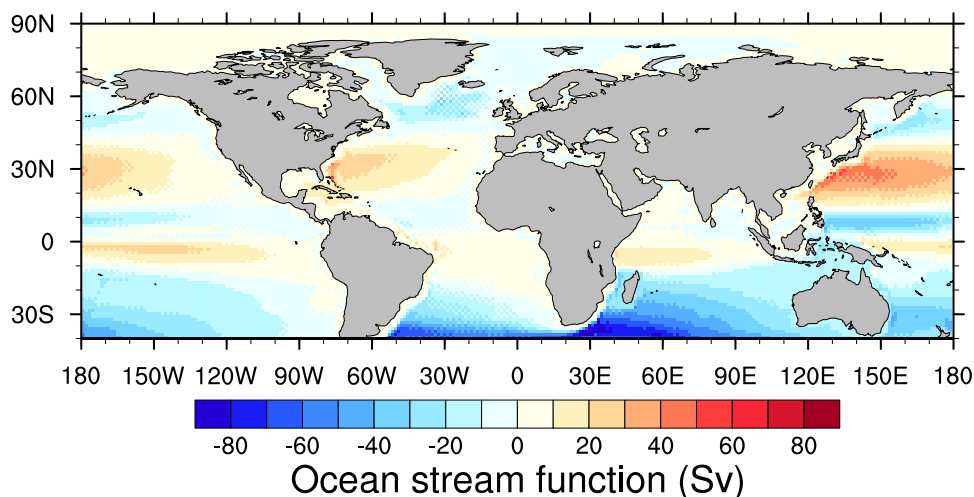
**Data availability** The climate model data presented in this paper are openly available from the University of Leeds Data Repository. <https://doi.org/10.5518/305>.

**Open Access** This article is distributed under the terms of the Creative Commons Attribution 4.0 International License (<http://creativecommons.org/licenses/by/4.0/>), which permits unrestricted use, distribution, and reproduction in any medium, provided you give appropriate credit to the original author(s) and the source, provide a link to the Creative Commons license, and indicate if changes were made.

## Appendix

The barotropic stream function in the ocean component of HadCM3 features a 2-grid wave structure in some regions of the world such as in the North Atlantic (Fig. 11). This

**Fig. 11** Ocean barotropic stream function (Sv) in the 9.5 ka simulation



feature is present in the pre-industrial control of the model as well as in each of our early Holocene simulations. It is believed to be a numerical artefact relating to the finite difference scheme and choice of diffusion time stepping used in the model. This artefact was present in the previous versions of HadCM3 (e.g. Born et al. 2013) and is not known to cause any serious issues in the ocean component of the model. HadCM3 has featured in multiple IPCC Assessment Reports (McAvaney et al. 2001; Randall et al. 2007; Flato et al. 2013) and has not been shown to behave in a wildly different way to other general circulation models in its simulated response over the North Atlantic to climate perturbations (e.g. Meehl et al. 2007). This gives us confidence that the model is able to simulate well the large scale features of the ocean circulation and the transport of water in the subpolar and subtropical gyres. However, some details of our calculations, such as quantitative changes in the Gulf Stream and ocean gyres should be interpreted with caution.

## References

- Beghin P, Charbit S, Dumas C, Kageyama M, Ritz C (2015) How might the North American ice sheet influence the northwestern Eurasian climate?. *Clim Past* 11:1467–1490. <https://doi.org/10.5194/cp-11-1467-2015>
- Berger A, Loutre MF (1991) Insolation values for the climate of the last 10 million years. *Quat Sci Rev* 10:297–317. [https://doi.org/10.1016/0277-3791\(91\)90033-Q](https://doi.org/10.1016/0277-3791(91)90033-Q)
- Born A, Stocker TF, Raible CC, Levermann A (2013) Is the Atlantic subpolar gyre bistable in comprehensive coupled climate models? *Clim Dyn* 40:2993–3007. <https://doi.org/10.1007/s00382-012-1525-7>
- Braconnot P, Marzin C, Grégoire L, Mosquet E, Marti O (2008) Monsoon response to changes in Earth's orbital parameters: comparisons between simulations of the Eemian and of the Holocene. *Clim Past* 4:281–294. <https://doi.org/10.5194/cp-4-281-2008>
- Cayan DR (1992) Latent and sensible heat flux anomalies over the northern oceans: driving the sea surface temperature. *J Phys Oceanogr* 22:859–881
- Cook KH, Held IM (1988) Stationary waves of the ice age climate. *J Clim* 1:807–819. <https://doi.org/10.1175/1520-0442%281988%29001%3C0807:SWOTIA%3E2.0.CO%3B2>
- Cox PM (2001) Description of the “TRIFFID” dynamic global vegetation model. *Hadley Cent Tech Note* 24:17
- Flato G, Marotzke J, Abiodun B, Braconnot P, Chou SC, Collins WJ, Cox P, Driouech F, Emori S, Eyring V, Forest C, Gleckler P, Guilyardi E, Jakob C, Kattsov V, Reason C, Rummukainen M (2013) Evaluation of climate models. *Climate change 2013: the physical science basis. Contribution of Working Group I to the Fifth Assessment Report of the Intergovernmental Panel on Climate Change*, in: climate change 2013. Cambridge University Press, pp 741–866
- Gong X, Zhang X, Lohmann G, Wei W, Zhang X, Pfeiffer M (2015) Higher Laurentide and Greenland ice sheets strengthen the North Atlantic ocean circulation. *Clim Dyn* 45:139–150. <https://doi.org/10.1007/s00382-015-2502-8>
- Gordon C, Cooper C, Senior CA, Banks H, Gregory JM, Johns TC, Mitchell JFB, Wood RA (2000) The simulation of SST, sea ice extents and ocean heat transports in a version of the Hadley Centre coupled model without flux adjustments. *Clim Dyn* 16:147–168. <https://doi.org/10.1007/s003820050010>
- Gregoire LJ, Payne AJ, Valdes PJ (2012) Deglacial rapid sea level rises caused by ice-sheet saddle collapses. *Nature* 487:219–222. <https://doi.org/10.1038/nature11257>
- Gregoire LJ, Valdes PJ, Payne AJ (2015) The relative contribution of orbital forcing and greenhouse gases to the North American deglaciation. *Geophys Res Lett* 42:2015GL066005. <https://doi.org/10.1002/2015GL066005>
- Gregoire LJ, Otto-Bliesner B, Valdes PJ, Ivanovic R (2016) Abrupt Bølling warming and ice saddle collapse contributions to the Meltwater Pulse 1a rapid sea level rise. *Geophys Res Lett*. <https://doi.org/10.1002/2016GL070356>
- Hall NMJ, Valdes PJ, Dong B, (1996) The maintenance of the Last Great Ice sheets: a UGAMP GCM study. *J Clim* 9:1004–1019. <https://doi.org/10.1175/1520-0442%281996%29009%3C1004:TMOTLG%3E2.0.CO%3B2>
- Held IM, Ting M, Wang H (2002) Northern winter stationary waves: theory and modeling. *J Clim* 15:2125–2144. <https://doi.org/10.1175/1520-0442%282002%29015%3C2125:NWSWT A%3E2.0.CO%3B2>
- Hillaire-Marcel C, de Vernal A, Piper DJW (2007) Lake Agassiz Final drainage event in the northwest North Atlantic. *Geophys Res Lett* 34:L15601. <https://doi.org/10.1029/2007GL030396>
- Hoskins BJ, Karoly DJ (1981) The steady linear response of a spherical atmosphere to thermal and orographic forcing. *J Atmos Sci* 38:1179–1196. <https://doi.org/10.1175/1520-0469%281981%29038%3C1179:TSLROA%3E2.0.CO%3B2>
- Hostetler SW, Clark PU, Bartlein PJ, Mix AC, Pisias NJ (1999) Atmospheric transmission of North Atlantic Heinrich events. *J Geophys Res Atmos* 104:3947–3952. <https://doi.org/10.1029/1998JD200067>
- Ivanovic RF, Valdes PJ, Flecker R, Gregoire LJ, Gutjahr M (2013) The parameterisation of Mediterranean–Atlantic water exchange in the Hadley Centre model HadCM3, and its effect on modelled North Atlantic climate. *Ocean Model* 62:11–16. <https://doi.org/10.1016/j.ocemod.2012.11.002>
- Ivanovic RF, Valdes PJ, Flecker R, Gutjahr M (2014) Modelling global-scale climate impacts of the late Miocene Messinian Salinity Crisis. *Clim Past* 10:607–622. <https://doi.org/10.5194/cp-10-607-2014>
- Ivanovic RF, Gregoire LJ, Kageyama M, Roche DM, Valdes PJ, Burke A, Drummond R, Peltier WR, Tarasov L (2016) Transient climate simulations of the deglaciation 21–9 thousand years before present (version 1)—PMIP4 Core experiment design and boundary conditions. *Geosci Model Dev* 9:2563–2587. <https://doi.org/10.5194/gmd-9-2563-2016>
- Ivanovic RF, Gregoire LJ, Wickert AD, Valdes PJ, Burke A (2017) Collapse of the North American ice saddle 14,500 years ago caused widespread cooling and reduced ocean overturning circulation. *Geophys Res Lett* 44:2016GL071849. <https://doi.org/10.1002/2016GL071849>
- Kageyama M, Valdes PJ (2000) Impact of the North American ice-sheet orography on the Last Glacial Maximum eddies and snowfall. *Geophys Res Lett* 27:1515–1518. <https://doi.org/10.1029/1999GL011274>
- Leher F, Born A, Raible CC, Stocker TF (2013) Amplified inception of European little ice age by sea ice–ocean–atmosphere feedbacks. *J Clim* 26:7586–7602. <https://doi.org/10.1175/JCLI-D-12-00690.1>
- Li C, Battisti DS (2008) Reduced Atlantic storminess during last glacial maximum: evidence from a coupled climate model. *J Clim* 21:3561–3579. <https://doi.org/10.1175/2007JCLI2166.1>
- Liakka J (2012) Interactions between topographically and thermally forced stationary waves: implications for ice-sheet evolution.

- Tellus Dyn Meteorol Oceanogr 64:11088. <https://doi.org/10.3402/tellusa.v64i0.11088>
- Liakka J, Nilsson J, Löffverström M (2012) Interactions between stationary waves and ice sheets: linear versus nonlinear atmospheric response. *Clim Dyn* 38:1249–1262. <https://doi.org/10.1007/s00382-011-1004-6>
- Liakka J, Löffverström M, Colleoni F (2016) The impact of the North American glacial topography on the evolution of the Eurasian ice sheet over the last glacial cycle. *Clim Past* 12:1225–1241. <https://doi.org/10.5194/cp-12-1225-2016>
- Liu Z, Otto-Bliesner BL, He F, Brady EC, Tomas R, Clark PU, Carlson AE, Lynch-Stieglitz J, Curry W, Brook E, Erickson D, Jacob R, Kutzbach J, Cheng J (2009) Transient simulation of last deglaciation with a new mechanism for Bølling–Allerød warming. *Science* 325:310–314. <https://doi.org/10.1126/science.1171041>
- Löffverström M, Lora JM (2017) Abrupt regime shifts in the North Atlantic atmospheric circulation over the last deglaciation. *Geophys Res Lett* 44:2017GL074274. <https://doi.org/10.1002/2017GL074274>
- Löffverström M, Caballero R, Nilsson J, Kleman J (2014) Evolution of the large-scale atmospheric circulation in response to changing ice sheets over the last glacial cycle. *Clim Past* 10:1453–1471. <https://doi.org/10.5194/cp-10-1453-2014>
- Löffverström M, Liakka J, Kleman J (2015) The North American Cordillera—an impediment to growing the continent-wide Laurentide ice sheet. *J Clim* 28:9433–9450. <https://doi.org/10.1175/JCLI-D-15-0044.1>
- Löffverström M, Caballero R, Nilsson J, Messori G (2016) Stationary wave reflection as a mechanism for zonalizing the Atlantic Winter jet at the LGM. *J Atmos Sci* 73:3329–3342. <https://doi.org/10.1175/JAS-D-15-0295.1>
- Loulergue L, Schilt A, Spahni R, Masson-Delmotte V, Blunier T, Lemieux B, Barnola J-M, Raynaud D, Stocker TF, Chappellaz J (2008) Orbital and millennial-scale features of atmospheric CH<sub>4</sub> over the past 800,000 years. *Nature* 453:383–386. <https://doi.org/10.1038/nature06950>
- Lunt DJ, Foster GL, Haywood AM, Stone EJ (2008) Late Pliocene Greenland glaciation controlled by a decline in atmospheric CO<sub>2</sub> levels. *Nature* 454:1102–1105. <https://doi.org/10.1038/nature07223>
- Matero ISO, Gregoire LJ, Ivanovic RF, Tindall JC, Haywood AM (2017) The 8.2 ka cooling event caused by Laurentide ice saddle collapse. *Earth Planet Sci Lett* 473:205–214. <https://doi.org/10.1016/j.epsl.2017.06.011>
- McAvaney BJ, Covey C, Joussaume S, Kattsov V, Kitoh A, Ogana W, Pitman AJ, Weaver AJ, Wood RA, Zhao Z-C (2001) Model evaluation, in: *climate change 2001: the scientific basis. Contribution of WG1 to the Third Assessment Report of the IPCC (TAR)*. Cambridge University Press, pp 471–523
- Meehl GA, Stocker TF, Collins WD, Friedlingstein AT, Gaye AT, Gregory JM, Kitoh A, Knutti R, Murphy JM, Noda A, Raper SCB, Watterson IG, Weaver AJ, Zhao Z (2007) Global climate projections. In: Soloman S, Qin D, Manning M, Marquis M, Averyt K, Tignor M.M.B., Miller HJ, Chen Z (eds) *Climate change 2007: the physical science basis. Contribution of Working Group I to the Fourth Assessment Report of the Intergovernmental Panel on Climate Change*. Cambridge University Press, Cambridge, pp 747–845
- Parrenin F, Barnola J-M, Beer J, Blunier T, Castellano E, Chappellaz J, Dreyfus G, Fischer H, Fujita S, Jouzel J, Kawamura K, Lemieux-Dudon B, Loulergue L, Masson-Delmotte V, Narcisi B, Petit J-R, Raisbeck G, Raynaud D, Ruth U, Schwander J, Severi M, Spahni R, Steffensen JP, Svensson A, Udisti R, Waelbroeck C, Wolff E (2007) The EDC3 chronology for the EPICA Dome C ice core. *Clim Past* 3:485–497. <https://doi.org/10.5194/cp-3-485-2007>
- Pausata FSR, Li C, Wettstein JJ, Kageyama M, Nisancioglu KH (2011) The key role of topography in altering North Atlantic atmospheric circulation during the last glacial period. *Clim Past* 7:1089–1101. <https://doi.org/10.5194/cp-7-1089-2011>
- Peltier WR (2004) Global glacial isostasy and the surface of the ice-age earth: the ice-5G (VM2) model and grace. *Annu Rev Earth Planet Sci* 32:111–149
- Peltier WR, Argus DF, Drummond R (2015) Space geodesy constrains ice age terminal deglaciation: the global ICE-6G\_C (VM5a) model. *J Geophys Res Solid Earth* 120:2014JB011176. <https://doi.org/10.1002/2014JB011176>
- Petit JR, Jouzel J, Raynaud D, Barkov NI, Barnola J-M, Basile I, Bender M, Chappellaz J, Davis M, Delaygue G, Delmotte M, Kotlyakov VM, Legrand M, Lipenkov VY, Lorius C, Pépin L, Ritz C, Saltzman E, Stievenard M (1999) Climate and atmospheric history of the past 420,000 years from the Vostok ice core. *Antarct Nat* 399:429–436. <https://doi.org/10.1038/20859>
- Pope VD, Gallani ML, Rowntree PR, Stratton RA (2000) The impact of new physical parametrizations in the Hadley Centre climate model: HadAM3. *Clim Dyn* 16:123–146. <https://doi.org/10.1007/s003820050009>
- Randall DA, Wood RA, Bony S, Colman R, Fichefet T, Fyfe J, Kattsov V, Pitman A, Shukla J, Srinivasan J (2007) Climate models and their evaluation, in: *climate change 2007: the physical science basis. Contribution of Working Group I to the Fourth Assessment Report of the IPCC (FAR)*. Cambridge University Press, pp 589–662
- Renssen H, Seppä H, Heiri O, Roche DM, Goosse H, Fichefet T (2009) The spatial and temporal complexity of the Holocene thermal maximum. *Nat Geosci* 2:411–414. <https://doi.org/10.1038/ngeo513>
- Renssen H, Goosse H, Crosta X, Roche DM (2010) Early Holocene Laurentide Ice Sheet deglaciation causes cooling in the high-latitude Southern Hemisphere through oceanic teleconnection. *Paleoceanography* 25:PA3204. <https://doi.org/10.1029/2009PA001854>
- Ringler TD, Cook KH (1999) Understanding the seasonality of orographically forced stationary waves: interaction between mechanical and thermal forcing. *J. Atmospheric Sci.* 56:1154–1174. [https://doi.org/10.1175/1520-0469\(1999\)056<1154:UTS OOF>2.0.CO;2](https://doi.org/10.1175/1520-0469(1999)056<1154:UTS OOF>2.0.CO;2)
- Roberts WHG, Valdes PJ, Payne AJ (2014) Topography's crucial role in Heinrich events. *Proc Natl Acad Sci* 111:16688–16693. <https://doi.org/10.1073/pnas.1414882111>
- Rodwell MJ, Rowell DP, Folland CK (1999) Oceanic forcing of the wintertime North Atlantic Oscillation and European climate. *Nature* 398:320–323. <https://doi.org/10.1038/18648>
- Semenov VA, Park W, Latif M (2009) Barents Sea inflow shutdown: a new mechanism for rapid climate changes. *Geophys Res Lett* 36:L14709. <https://doi.org/10.1029/2009GL038911>
- Singarayer JS, Valdes PJ (2010) High-latitude climate sensitivity to ice-sheet forcing over the last 120 kyr. *Quat Sci Rev* 29:43–55. <https://doi.org/10.1016/j.quascirev.2009.10.011>
- Singarayer JS, Valdes PJ, Friedlingstein P, Nelson S, Beerling DJ (2011) Late Holocene methane rise caused by orbitally controlled increase in tropical sources. *Nature* 470:82–85. <https://doi.org/10.1038/nature09739>
- Spahni R, Chappellaz J, Stocker TF, Loulergue L, Hausammann G, Kawamura K, Flückiger J, Schwander J, Raynaud D, Masson-Delmotte V, Jouzel J (2005) Atmospheric methane and nitrous oxide of the late pleistocene from Antarctic Ice cores. *Science* 310:1317–1321. <https://doi.org/10.1126/science.1120132>
- Tarasov L, Dyke AS, Neal RM, Peltier WR (2012) A data-calibrated distribution of deglacial chronologies for the North American ice complex from glaciological modeling. *Earth Planet Sci Lett* 315–316:30–40. <https://doi.org/10.1016/j.epsl.2011.09.010>

- Teller JT, Leverington DW, Mann JD (2002) Freshwater outbursts to the oceans from glacial Lake Agassiz and their role in climate change during the last deglaciation. *Quat Sci Rev* 21:879–887. [https://doi.org/10.1016/S0277-3791\(01\)00145-7](https://doi.org/10.1016/S0277-3791(01)00145-7)
- Valdes PJ, Hoskins BJ (1991) Nonlinear orographically forced planetary waves. *J Atmos Sci* 48:2089–2106. <https://doi.org/10.1175/1520-0469%281991%29048%3C2089:NOFPW%3E2.0.CO%3B2>
- Valdes PJ, Armstrong E, Badger MPS, Bradshaw CD, Bragg F, Davies-Barnard T, Day JJ, Farnsworth A, Hopcroft PO, Kennedy AT, Lord NS, Lunt DJ, Marzocchi A, Parry LM, Roberts WHG, Stone EJ, Tourte GJL, Williams JHT (2017) The BRIDGE HadCM3 family of climate models: HadCM3@Bristol v1.0. *Geosci Model Dev Discuss.* <https://doi.org/10.5194/gmd-2017-16>
- Vellinga M, Wood RA, Gregory JM (2002) Processes governing the recovery of a perturbed thermohaline circulation in HadCM3. *J Clim* 15:764–780. [https://doi.org/10.1175/1520-0442\(2002\)015<0764:PGTROA>2.0.CO;2](https://doi.org/10.1175/1520-0442(2002)015<0764:PGTROA>2.0.CO;2)
- Xie S-P, Philander SGH (1994) A coupled ocean–atmosphere model of relevance to the ITCZ in the eastern Pacific. *Tellus A* 46:340–350
- Zhang X, Lohmann G, Knorr G, Purcell C (2014) Abrupt glacial climate shifts controlled by ice sheet changes. *Nature* 512:290–294. <https://doi.org/10.1038/nature13592>